Two-step oxygen injection process for growing ZnO nanorods

Yung-Kuan Tseng
Materials Research Laboratories, Industrial Technology Research Institute, Bldg. 77, 195 Section 4 Chung Hsing Road, Chutung, Hsinchu 310, Taiwan, Republic of China

Hsu-Cheng Hsu and Wen-Feng Hsieh
Institute of Electro-Optical Engineering, National Chiao Tung University, 1001 Tahsueh Road, Hsinchu 300, Taiwan, Republic of China

Kuo-Shung Liu
Department of Material Science and Engineering, National Tsing-Hua University, 101, Section 2 Kuang Fu Road, Hsinchu 300, Taiwan, Republic of China

I-Cherng Chen[a)]
Materials Research Laboratories, Industrial Technology Research Institute, Bldg. 77, 195 Section 4 Chung Hsing Road, Chutung, Hsinchu 310, Taiwan, Republic of China

(Received 9 June 2003; accepted 15 September 2003)

Uniform hexagonal prismatic zinc oxide rods were grown over the entire alumina substrate at 550 °C using a two-step oxygen injection process, whether the substrates were coated with a catalyst or not. X-ray diffraction showed that all of the depositions exhibited a preferred orientation in the (002) plane. The influence of oxygen concentration was investigated by changing the oxygen flow rate. Oxygen concentration affected the size of ZnO nanorods, especially the diameter. The ZnO nanorods were further checked using high-resolution transmission electron microscopy, photoluminescence, Raman spectroscopy, and room-temperature ultraviolet lasing. The results showed that the rods were single crystals and had excellent optical properties. By observing the growth process, we found that the diameter increased slowly, but the longitudinal growth rate was very high. The growth of ZnO nanorods revealed that the uniform hexagonal prismatic ZnO nanorods were synthesized through vapor deposition growth and a self-catalyzed vapor–liquid–solid (VLS) process.

I. INTRODUCTION

Semiconductor one-dimensional (1D) nanostructures have attracted much attention in recent years, especially in mesoscopic research and due to their potential application in manufacturing nanodevices. The main reasons for this are their interesting photonic and electronic properties, and their importance as a building block for interconnects of transistors, junctions of metal-semiconductors, and the tips of emitters. Many studies have been carried out on the whiskers and wires of Si and III-V systems[1–9] as well as on the oxide systems, including SnO2,[10] SiO2,[11] GeO2,[12] ZnO,[13–15] indium tin oxide (ITO),[16] and Al_2O_3.[17] Among them, ZnO is an *n*-type semiconductor with a wide-band gap (3.30 eV). It emits short-wavelength light, shows piezoelectric properties, and is transparent in the visible range. It is also electrically conductive with appropriate dopants such as Al, Ga, In, Sn, etc. Huang *et al.*[18] reported the successful gas phase synthesis of ZnO nanowires on patterned Au catalyst by the vapor–liquid–solid (VLS) reaction. They used carbothermal or hydrogen reduction of ZnO as a zinc vapor source at 900–925 °C. Pan *et al.*[19] synthesized ZnO nanobelts by thermal evaporation of ZnO powder at 1400 °C. The low-temperature gas phase processes have also been reported. Park *et al.*[20] used a metalorganic vapor-phase epitaxy method to grow ZnO nanorods at 400 °C without a metal catalyst. Wu *et al.*[21] deposited ZnO nanorods on fused silica substrates by thermal chemical vapor deposition (CVD) at around 500 °C. Lyu *et al.*[22] used NiO as a catalyst and Zn powder as a vapor source to synthesize ZnO nanowires through metal-vapor deposition at 450 °C. Tseng *et al.*[23] demonstrated the feasibility of selected-area growth of ZnO nanowires at low temperature (500 °C) via the VLS synthesis mechanism. According to these findings, the growth temperature of single crystal ZnO nanowires could be formed at as low as 400 °C through to as high as 1300 °C. Synthesizing single-crystal ZnO nanowires at low temperature not only reduces the heat budget, but also combines

[a)]Address all correspondence to this author.
e-mail: EugeneChen@itri.org.tw

the ZnO nanostructures with manufacturing microelectric processing, because the growth at low temperatures would reduce the phase transformation of the materials and the interdiffusion between the deposited layers. Generally speaking, the temperature of the manufacturing microelectric processing is lower than 550 °C. For this reason, the growth temperature was lower than 550 °C in our studies.

Based on our trials to synthesize zinc oxide rods at 550 °C, we found that it is effective to grow zinc oxide nanorods by supplying oxygen into the reaction system in a two-step process. In this study, we will report a two-step oxygen injection method for growing uniform hexagonal prismatic zinc oxide nanorods. We have tested various oxygen flow rates to find the optimal growth condition. Moreover, using this two-step inflowing oxygen gas process could result in the production of zinc oxide rods on the alumina substrates without catalysts. The ZnO nanorods, which were grown under optimal conditions, were further investigated through their optical properties and structural characteristics. We also took samples during the synthesis process to observe the growth of ZnO nanorods and to discuss the growth mechanism. We believe that uniform hexagonal prismatic ZnO nanorods were synthesized due to vapor deposition growth and a self-catalyzed VLS process.

II. EXPERIMENTAL

Figure 1 schematically depicts the low-pressure chemical vapor transport and deposition system used for growing ZnO nanorods. To study the growth steps of the ZnO rods during the synthesis process, this chamber has sampling tappets and valves by which the direction of gas flow can be controlled. Zn metal powder (99.9% 300 mesh, Strem Chemicals, Newburyport, MA) was placed in an alumina oxide boat. The alumina substrates were thick film grade (purity is 96%). Some substrates were deposited with a 30–50 Å thin layer of Au as catalyst by direct current sputtering. The zinc vapor source and substrates were put into a quartz tube with a length of 20 mm. The zinc vapor source was placed on the upstream side.

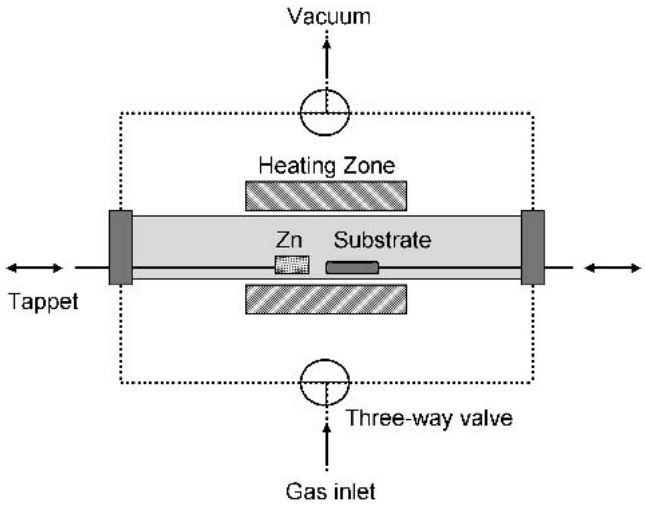

FIG. 1. Low-pressure chemical vapor transport and deposition system with tappets for investigating the synthesis of ZnO nanowires.

A mechanical pump was used to evacuate the system to maintain the pressure inside the quartz tube at about 10 torr. A programmable temperature controller was used to keep the heating ramp at 20 °C per minute. The reaction gases were directed into the reaction system in two steps by mass flow controllers. The first step was to lead an argon flow of 54 sccm into the reaction system as the experiment began. When the furnace temperature reached 420 °C, an oxygen flow of 0–3 sccm was added into the argon flow as the second step, until the end of experiment. The crystalline structure of the samples was analyzed by using an x-ray diffraction (XRD) Philips PW3710 diffractometer and a transmission electron microscope (TEM; JEOL, JEM-2000FX, operated at 200 KV). The morphology and size distribution were characterized using a field emission scanning electron microscope (FE-SEM; LEO 1530, operated at 5KeV) (LEO Electron Microscopy, Oberkochen, Germany). A Jobin Yvon-Spex fluorolog-3 spectrophotometer was used to conduct the photoluminescence studies. Raman spectroscopy measurements were carried out at room temperature in the backscattering geometry using a Dilor X-Y modular laser Raman spectrometer. This spectrometer uses a Ar ion laser with a wavelength of 514.5 nm (2.41 eV).

III. RESULTS AND DISCUSSION

A. Two-step oxygen injection process with various oxygen flow rates

In our experiments, oxygen was the only oxidizer in the synthesis. Therefore, the quantity of oxygen and the timing of its flow into the reaction system would affect the deposition of zinc oxide. During our trials of synthesizing zinc oxide rods at 550 °C, we found that leading oxygen into the reaction system when the temperature was raised above 400 °C, especially 420 °C, is an effective strategy to grow uniform hexagonal prismatic zinc oxide rods.

Based on the two-step reaction gas injection process, the influence of oxygen concentration was investigated at flow rates of 0.2, 0.6, 1.0, 2.0, and 3.0 sccm. Experiments were conducted at 550 °C for 30 min with a coated gold alumina substrate. Argon flow of around 54–55 sccm was led into the synthesis system to maintain the vacuum pressure at 10 torr. The results were examined by FE-SEM. As shown in Fig. 2, the results from various oxygen flow rates demonstrated that the growth of zinc

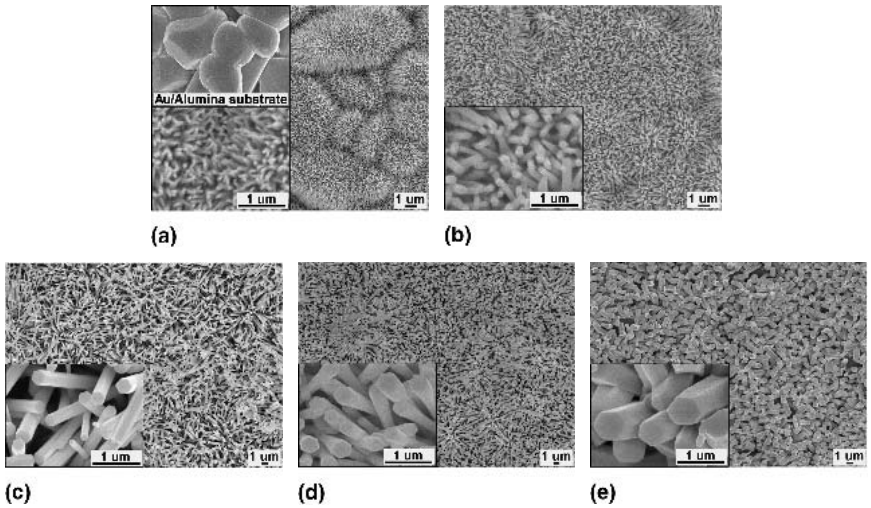

FIG. 2. FE-SEM micrographs of the results from the two-step oxygen injection method for deposition zinc oxide rods on coated gold alumina substrates with various oxygen flow rates of (a) 0.2 sccm, (b) 0.6 sccm, (c) 1.0 sccm, (d) 2.0 sccm, and (e) 3.0 sccm. The insets at lower left corner show the same sample at a higher magnification. The inset at higher left corner in (a) is the image of fresh coated gold alumina substrate.

oxide nanorods was over the entire surface of the alumina substrate. In addition, the size of the nanorods increased as the flow rates increased. The results were further checked with XRD. The XRD spectra in Fig. 3 show the depositions were all pure wurtzite-type ZnO.[24] The sharp peaks and the special strong (002) peak indicate that the nanorods had good crystallinity and a growth orientation of [001], as reported by other groups.[25]

The size distribution of zinc nanorods is illustrated in Fig. 4. It shows that the diameter and length of ZnO nanorods increased with oxygen flow rate. The diameter grows at a slower rate than the length. We also found that there exists a nearly proportional relationship between the oxygen flow rate and the longitudinal growth rate of the rods. As the flow rate increased from 0.2 to 0.6 sccm, the length of the nanorods was approximately doubled. Similarly, the length at 1.0 sccm was twice the length at 0.6 sccm. However, when the flow rate was greater than 1.0 sccm, the diameter still increased but the length almost stopped increasing. Therefore, oxygen concentration could be used to control the size of ZnO nanorods, especially the diameter.

The oxygen concentration not only affects the growth rate, but also the crystallinity. Figure 5 shows the photoluminescence (PL) measurements of different oxygen flow rates. The green emission at about 490 nm is related to the singly ionized oxygen vacancy[22,26] and only appeared as the oxygen flow rate was smaller than 1 sccm. This could be explained as the oxidization efficiency. When the oxygen concentration is low, the probability of making the zinc atom become oxidized and bonded to the surface is low. Thus, a low oxygen concentration not only causes a low growth rate but also more oxygen vacancy defects. On the contrary, a high oxygen concentration was helpful to the formation of zinc–oxygen

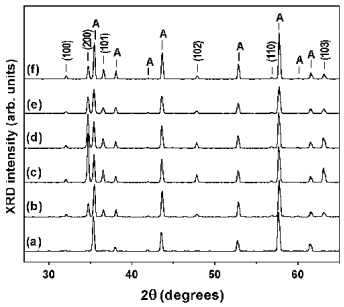

FIG. 3. XRD spectra ($2\theta = 27°$ to 65°) of the results from the deposition of zinc oxide rods on coated gold alumina substrates with various oxygen flow rates of (a) 0.2 sccm, (b) 0.6 sccm, (c) 1.0 sccm, (d) 2.0 sccm, (e) 3.0 sccm, and on bare alumina substrates with an oxygen flow rate of (f) 1.0 sccm. (A: peaks of alumina substrates.)

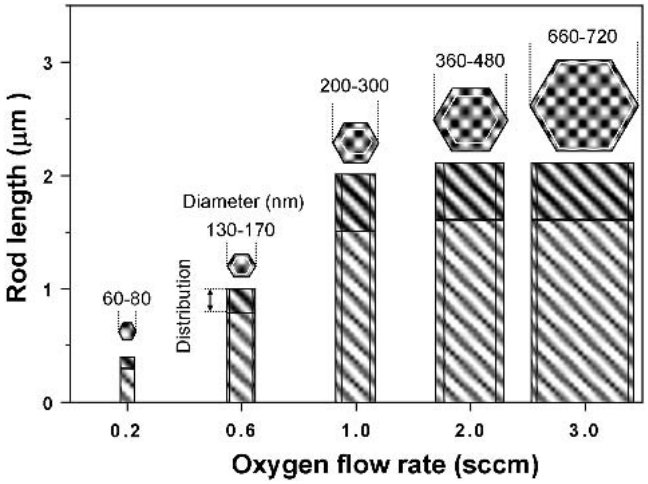

FIG. 4. The size distributions of the zinc oxide rods which deposited on the coated gold alumina substrates with various oxygen flow rates.

bonds. For that reason, the oxygen vacancy defects decreased and the crystal growth speeded up. Consequently, oxygen concentration would affect the size and crystallinity of the ZnO nanorods.

B. Further structure characterization and optical properties of the ZnO nanorods grown under the optimal conditions

Well-defined hexagonal ZnO nanorods were also grown all over the bare alumina substrate with an oxygen flow of 1 sccm at 550 °C (Fig. 6). The nanorods had a diameter of 200–300 nm and a length of 1.5–2.0 μm, which was virtually the same as that grown on the coated gold substrate [Fig. 2(c)]. The XRD spectrum of the deposition on the bare alumina substrate also shows the sharp peaks and the special strong preferred (002) peak [Fig. 3(f)]. These facts indicate that gold catalyst is not necessary for the growth of ZnO nanorods.

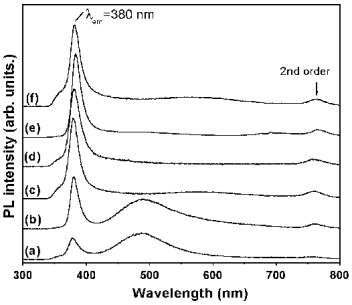

FIG. 5. Room-temperature PL emission spectra of the results from the deposition of zinc oxide rods on coated gold alumina substrates with various oxygen flow rates of (a) 0.2 sccm, (b) 0.6 sccm, (c) 1.0 sccm, (d) 2.0 sccm, (e) 3.0 sccm., and on bare alumina substrates with an oxygen flow rate of (f) 1.0 sccm. These were excited at $\lambda_{exc} = 254$ nm.

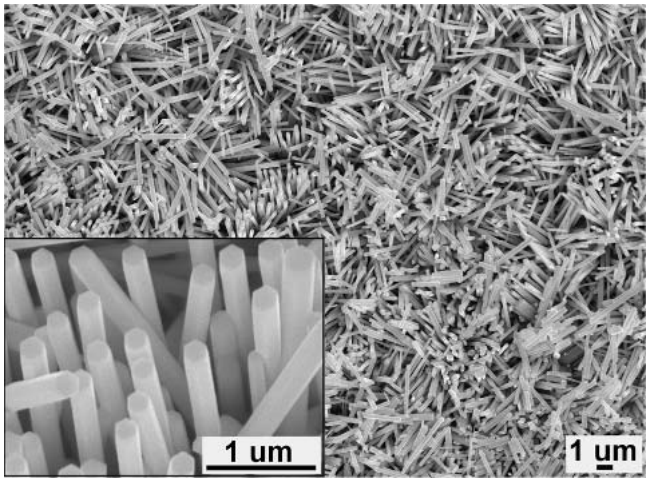

FIG. 6. FE-SEM micrographs of the results from the two-step oxygen injection method for depositing zinc oxide rods on the bare alumina substrates at 550 °C. The insets show the same sample at a higher magnification.

The Raman spectra of the ZnO nanorods grown on bare alumina substrate and coated gold alumina substrate are both shown in Fig. 7. The spectrum of the sample grown on the coated gold alumina substrate suggests a strong fluorescence background, which should be induced from gold. Both samples, either with or without gold catalyst, showed a strong peak at 437 cm^{-1}, which corresponds to the E_2 mode of ZnO crystal. This is apparently the contribution from the ZnO nanorods.[27,28] In addition, the small peak of the E_1 longitudinal optical phonon (LO) mode of ZnO crystal at 583 cm^{-1}, which is associated with oxygen deficiency,[29] indicates the existence of oxygen defects.

The optical properties of the ZnO nanowires on bare alumina substrates and coated gold alumina substrate were compared using PL spectroscopy with ultraviolet ($\lambda_{exc} = 254$ nm). Figures 5(c) and (f) were the spectra obtained from the ZnO nanowires grown on bare alumina substrate and on coated gold alumina substrate respectively. They are almost the same. The dominant peak was observed at approximately 380 nm. It is attributed to the recombination of free excitons through an exciton–exciton collision process,[22] which is the 3.3 eV (376 nm) wide direct band gap transition of ZnO nanowires at room temperature.[30,31] A weak and broad green band (510–580 nm) is observed and almost negligible. It has been suggested that the green band emission corresponds to the singly ionized oxygen vacancy in ZnO.[22] For that reason, this green band indicates a very low concentration of oxygen vacancy in the ZnO nanorods. This is observed in the Raman spectrum in the same way as the weak E_2 mode peak of ZnO crystal. In summary, these results reveal the ZnO nanorods grown on bare alumina substrate and coated gold alumina substrate are also of high optical quality.

Huang *et al.*[32] have reported single-crystalline, well-faceted ZnO nanorods, which can function as self-contained optical resonance cavities, and demonstrated lasing action at room temperature. Using pumped lasing on ZnO nanorods is a good indicator of crystal quality. Therefore, we used the third harmonic of a Nd:YVO_4 laser (3.51 eV photon energy) as the pump source which

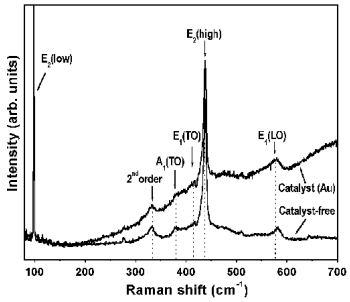

FIG. 7. Raman spectra of the ZnO nanorods grown on bare alumina substrate and coated gold alumina substrate.

has pulse width of approximately 500 ns pulse and a repetition rate of 1kHz. The excitation laser beam was focused onto the sample surface. Spontaneous and stimulated emissions were collected and coupled into a 32 cm monochromator with a 1200 line/mm grating, and it was detected by an electrically cooled charge-coupled device camera. The optical pumping experiments were carried out at room temperature.

Figure 8 shows typical lasing spectra of Au-catalyzed and catalyst-free nanorods at the same pumping density. Figure 8(a) presents the variations of the intensity of light emitted in a range of pump pulse energies at 386 nm. A lasing threshold is observed at 4 μJ, corresponding to an intensity of 2 MW/cm^2. Figure 8(b) shows the above lasing threshold of Au-catalyzed and catalyst-free nanorods with the same pumping density of 9 μJ (5 MW/cm^2). A strong and narrow stimulated emission peak with a full width at half-maximum of 3 nm appears on the long-wave side of the PL spectrum and is similar to such peaks found by other research groups[33,34] using ZnO films. The result indicates that the emission peak caused by results from inelastic exciton–exciton scattering and the natively formed the ZnO nanorods serve as the Fabry–Perot cavity. The samples in this work exhibit unclear Fabry–Perot modes unlike those in previous reports of lasing from ZnO nanowires.[32,35] This finding may follow from the fact that the measured stimulated emission spectra are averages over ZnO nanorods with various lengths within the pumping area. The superposition of the individual emission spectra from ZnO nanorods with cavities of different lengths causes the Fabry–Perot modes to overlap to form a broad lasing peak. The lasing threshold for the nanorods herein is higher than that obtained by Yang *et al.*,[32] perhaps because of the relatively strong light scattering from the rough facet of the bottom of the ZnO nanorods, as shown in Fig. 9. Photons escape from the rough end of the cavity; therefore, the required pumping intensity was higher in this study.

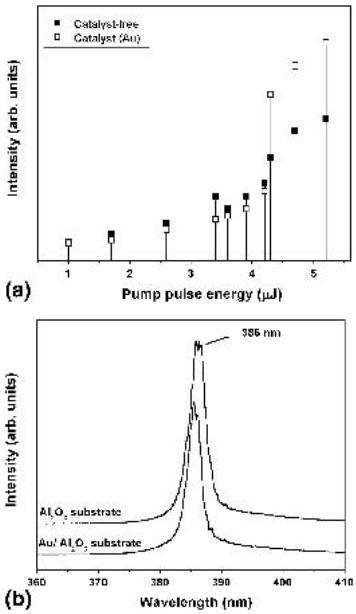

FIG. 8. (a) Peak intensity of optical emission at the 386 nm with various pump laser pulse energies by the Nd:YVO_4 laser. (b) Lasing spectra of the Au-catalyzed and catalyst-free nanorods pumped with excitation intensity of 5 MW/cm^2.

The structure characterization of the ZnO nanorods grown on the coated gold alumina substrate was assessed by high-resolution transmission microscopy (Fig. 10). The results of lattice fringes and the electron diffraction pattern confirmed that the nanorod is a single crystal. The lattice spacing of approximately 2.6 Å between adjacent lattice planes corresponded to the distance between two (002) crystal planes. This confirms [001] as the preferred growth direction for ZnO nanowires. The energy depressive x-ray analysis (EDX) on the nanorods showed that the composition was zinc and oxygen only. Within the detection limit of the EDX spectroscopy, there is no indication that Au atoms diffused into rods from the gold layer.

C. Observation of the growth process

During the synthesis process, we sampled using the tappets to observe the growth process. The experiment proceeded with the coated gold substrate maintained under optimal experimental conditions (O_2 = 1 sccm, 550 °C). The temperature profile and sampling time are shown in Fig. 11. Series samples at six conditions (440 °C, 480 °C, 520 °C, 550 °$C_{0\ min}$, 550 °$C_{5\ min}$, and 550 °$C_{10\ min}$) were collected.

The samples examined by FE-SEM and XRD are shown in Figs. 12 and 13, respectively. As shown by FE-SEM, some tiny particles appeared on the surface at 440 °C. When the temperature was raised to 480 °C, some small humps and larger particles were deposited on

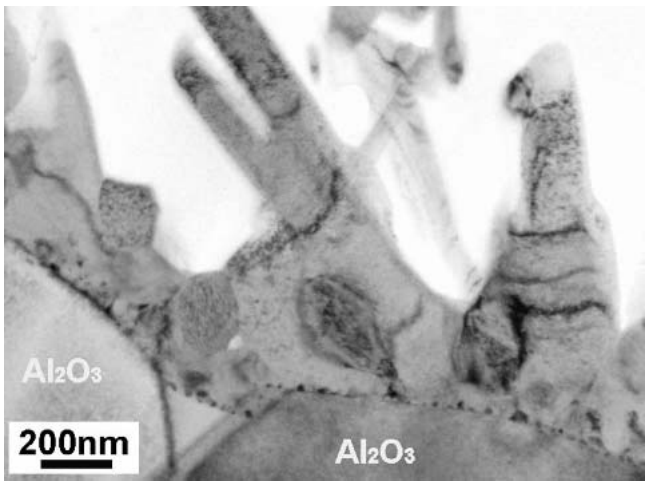

FIG. 9. TEM image of the cross-sectional sample of the ZnO nanorods grown on the coated gold alumina substrate.

the surface. No crystal phase was identified by XRD except for α-alumina coming from the substrate. However, zinc was detected by EDX analysis. As the temperature increased to 520 °C, the humps of 70 nm were grown over the entire substrate. Within only 1.5 min, the temperature reached 550 °C. The humps grew rapidly to rods with diameters of 70–160 nm and a length of 0.6 μm. After 5 min, the rods had a definite hexagonal shape and the length increased to 0.7–1.0 μm. However, the size distribution of the diameter returned virtually constant. Ten minutes later, the rods had only lengthened by a small amount to 0.8–1.3 μm. The longitudinal growth decreased obviously. The whole growth process of ZnO nanorods is depicted in Fig. 11. Briefly, the lateral growth rate is very low, but the longitudinal growth rate is very high—up to 80 nm per minute—while the temperature is maintained at 550 °C. The trend of the growth was consistent with the variation of the intensity of the ZnO(002) XRD peaks.

D. Mechanism of ZnO nanorod growth

Given that 1-D crystals grow essentially in one direction, their growth has been explained by the Frank mechanism[36] and VLS mechanism. The Frank mechanism is based on screw dislocation, which emerges at the growth interface. A screw dislocation provides a self-perpetuation step for the addition of new layers. The spiral plane perpendicular to the screw dislocation line possesses a step as a low-energy site for growth. The growth rate along the dislocation line is then much faster than that of the radius direction. Therefore, a crystal has

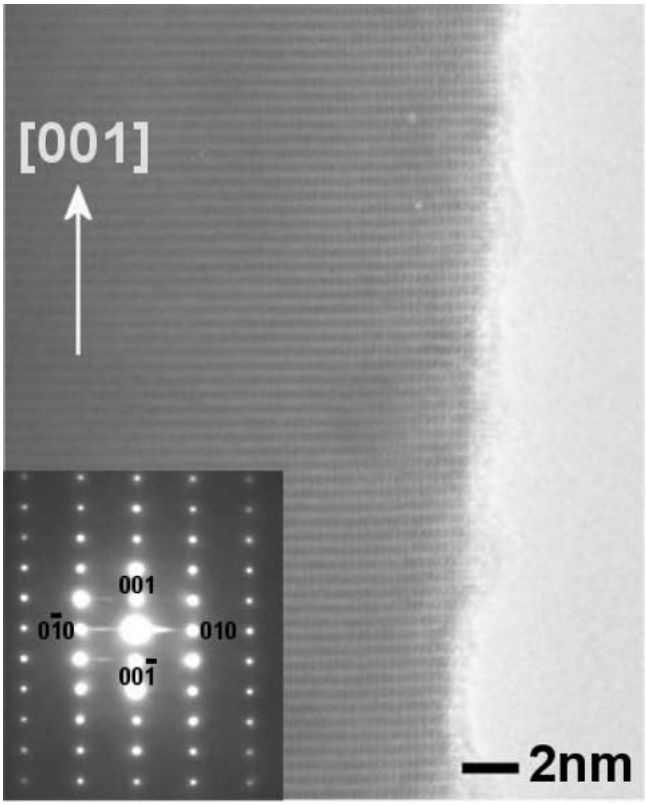

FIG. 10. High-resolution TEM image of an individual ZnO nanowire shows its [001] growth direction. The inset shows the corresponding selected-area electron diffraction from the nanorods.

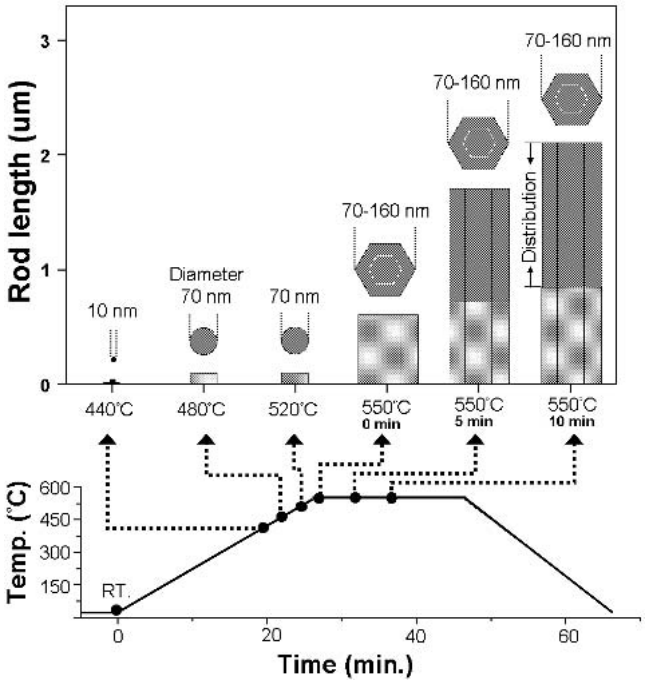

FIG. 11. The reaction temperature profile and sampling times, and the size distribution of the samples.

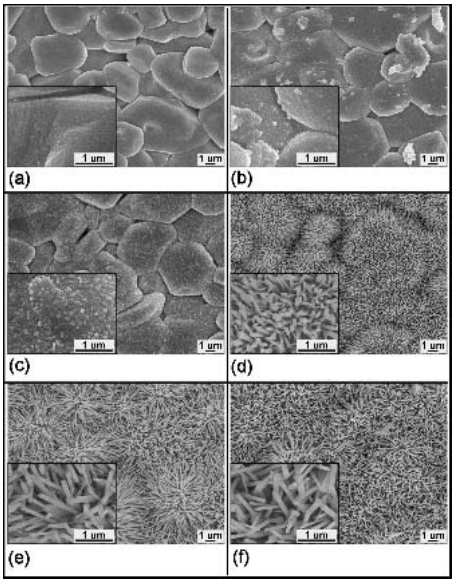

FIG. 12. FE-SEM micrographs of the results sampled during the deposition process at different temperatures and times as (a) 440 °C, (b) 480 °C, (c) 520 °C, (d) 550 °C (0 min.), (e) 550 °C (5 min.), and (f) 550 °C (10 min.).

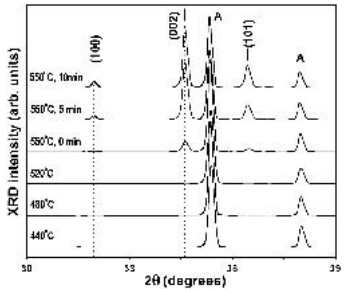

FIG. 13. XRD profiles of the results sampled during the deposition process at different temperatures and times.

a conic tip with spiral morphology at the end of the 1D structure and a screw dislocation, which runs parallel to the axis of the 1D structure. This is evidence for the Frank mechanism. However, based on the FE-SEM images (Figs. 2, 6, and 12) of our study, only well-faceted prismatic morphology is observed on the tops of ZnO nanorods. This indicates that the growth of ZnO nanorods did not follow the Frank mechanism in this study.

VLS growth uses nano-sized metal clusters as catalysts to absorb the gas-phase reactants and form eutectic alloy droplets. As the concentration of reactant in the liquidized droplets becomes oversaturated, precipitation begins, and the 1D structure is formed. The characteristic of the VLS growth is the existence of nanoparticles capped at the end of the 1D structure. In this study, Au metal was used as catalyst, but no additional metal particle appeared on the top or bottom of the nanowires, as shown in all the FE-SEM images (Figs. 2, 6, and 12) and the TEM image of the cross-sectional sample (Fig. 9). Furthermore, the ZnO nanorods were also grown on the bare alumina substrates. These observations from our experiments are not consistent with the features of VLS deposition.

Hu *et al.*[37] proposed a model called self-catalyzed VLS growth. They suggested that the vaporized Zn is deposited in the form of a liquid droplet. The liquidized zinc serves as a seed for ZnO whisker growth. The Zn droplets then react with O_2 to form ZnO. Because the ZnO melting temperature is 1975 °C,[38] the formation of ZnO on the Zn liquidized droplets is like the VLS mechanism. Zn not only acts as the reactant but also provides an energetically favored site for the absorption of O_2. Therefore, it could perform without any additional transition metal as catalyst.

Yao *et al.*[39] have a similar opinion. However, they believe that Zn suboxides play the same role for the nucleation of ZnO nanowires as Zn because both Zn and Zn suboxides have low melting temperatures (approximately 419 °C for both Zn and ZnO_x, where $x < 1$).[40]

We also found that Zn-rich composition existed in the sample. EDX analysis of a cross-sectional TEM sample (Fig. 9), revealed a composition that varied from near the interface of the ZnO and the alumina substrate to the root of the rod, from high Zn concentration to low Zn concentration, respectively. We believe that the gradient of zinc concentration is related to the two-step oxygen injection process.

Therefore, two-step oxygen injection is proposed as a growth mechanism for ZnO nanorods. At a low temperature, the atmosphere in the low-pressure-CVD system included only argon. Zinc atoms were vaporized from the zinc metal source and then deposited on the substrate to form clusters of zinc. When the temperature exceeded 420 °C, zinc clusters melted into droplets. The surface of the droplets had a high sticking coefficient and was therefore preferred site of absorption for zinc vapor.[10] Then, oxygen was directed into the reaction system, causing the droplets to be oxidized. The solubility of ZnO in liquidized Zn is very low,[40] so the ZnO molecules in the droplet precipitated out. A lower index crystal plane has a lower surface energy, so the ZnO molecules are arranged on the (001) crystal plane. In such a way, a proper cation–anion coordination is preserved to balance the local charge and structural symmetry,[41] such that the growth in the ⟨001⟩ direction was faster than that in the ⟨101⟩ and ⟨100⟩ directions.[42] Therefore, the ZnO nanorods grew quickly from the Zn droplets in the ⟨001⟩ direction by self-catalyzed VLS mechanism. As the rods lengthened, zinc and oxygen atoms also stuck onto the steps, ledges and kinks on the surface of the crystal to generate a flat plane and reduce the surface energy. Thus, the facets of the ZnO nanorods between the ⟨001⟩, and the ⟨100⟩ directions gradually disappeared. The (001) and (100) planes are the most likely to retain facets after the growth. Hence, well-faceted prismatic ZnO single crystals were formed on the substrate. However, the zinc vapor source (zinc metal powder) was depleted, and the Zn droplets were oxidized continuously. These resulted in the amount of liquidized Zn in the droplets gradually decreased, and the growth rate of the ZnO nanorods reduced in the final stage. This model could explain the observations of ZnO growth herein.

IV. CONCLUSIONS

Based on the two-step oxygen injection process, oxygen was led into reaction at 420 °C to grow zinc oxide nanorods. Uniform hexagonal prismatic zinc oxide rods were grown effectively over the entire alumina substrate at 550 °C, whether the alumina substrates was coated with gold or not. Using XRD, all of the depositions showed a preferred-orientation in the (002) plane. The effects of oxygen concentration were investigated by changing the flow rate. Briefly, when the oxygen flow rate increased, the diameters and lengths of ZnO nanorods increased. The rate of increase of the diameter is greater than that of the length. Therefore, oxygen

concentration could be used to control the size of ZnO nanorods, especially the diameter. In addition, our PL analysis indicated that higher oxygen concentration corresponded to better crystallinity of the ZnO nanorods.

The ZnO nanorods grown on the bare alumina substrate and coated gold alumina substrate with an oxygen flow of 1 sccm at 550 °C were further checked by high-resolution transmission electron microscopy, PL, Raman spectroscopy, and room-temperature UV lasing. The results showed that the rods were single crystals and had excellent optical properties.

From observing the growth process, we found that the diameter increased slowly. However, the longitudinal growth was fast with a rate of approximately 80 nm per minute while the temperature was maintained at 550 °C.

Our observation of the growth of ZnO nanorods revealed that the uniform hexagonal prismatic ZnO nanorods were synthesized through vapor deposition growth and a self-catalyzed VLS process.

REFERENCES

1. R.S. Wagner and W.C. Ellis, Appl. Phys. Lett. **4,** 89 (1964).
2. E.I. Givargizov, J. Cryst. Growth **32,** 20 (1975).
3. A.M. Morales and C.M. Lieber, Science **279,** 208 (1998).
4. S.T. Lee, N. Wang, and C.S. Lee, Mater. Sci. Eng. A **286,** 16 (2000).
5. C.C. Chen and C.C. Yeh, Adv. Mater. **12,** 738 (2000).
6. J. Zhu and S. Fan, J. Mater. Res. **14,** 1175 (1999).
7. M. Yazawa, M. Koguchi, A. Muto, M. Ozawa, and K. Hiruma, Appl. Phys. Lett. **60,** 2051 (1992).
8. X.F. Duan and C.M. Lieber, Adv. Mater. **279,** 208 (2000).
9. Y. Homma, P. Finnie, T. Ogino, H. Noda, and T. Urisu, J. Appl. Phys. **86,** 3083 (1999).
10. Z.R. Dai, Z.W. Pan, and Z.L. Wang, Adv. Funct. Mater. **13,** 9 (2003).
11. Y.Q. Zhu, W.B. Hu, W.K. Hsu, M. Terrones, N. Grobert, J.P. Hare, H.W. Kroto, D.R.M. Walton, and H. Terrones, J. Mater. Chem. **9,** 3173 (1999).
12. Z.G. Bai, D.P. Yu, H.Z. Zhang, Y. Ding, X.Z. Gai, Q.L. Hang, G.C. Xiong, and S.Q. Feng, Chem. Phys. Lett. **303,** 311 (1999).
13. K.F. Nielsen, J. Cryst. Growth **3–4,** 141 (1968).
14. S.D. Sharma and S.C. Kashyap, **42,** 5302 (1971).
15. J.Y. Li, X.L. Chen, H. Li, M. He, and Z.Y. Qiao, J. Cryst. Growth **233,** 5 (2001).
16. H. Yumoto, T. Sako, Y. Gotoh, K. Nishiyama, and T. Kaneko, J. Cryst. Growth **203,** 136 (1999).
17. V. Valcarcel, A. Souto, and F. Guitian, Adv. Mater. **10,** 138 (1998).
18. M.H. Huang, Y. Wu, H. Feick, N. Tran, E. Weber, and P. Yang, Adv. Mater. **13,** 113 (2000).
19. Z.W. Pan, Z.R. Dai, and Z.L. Wang, Science **291,** 1947 (2001).
20. W.I. Park, D.H. Kim, S-W. Jung, and G-C. Yi, Appl. Phys. Lett. **80,** 4232 (2002).
21. J.J. Wu and S-C. Liu, Adv. Mater. **14,** 215 (2002).
22. S.C. Lyu, Y. Zhang, H. Ruh, H-J. Lee, H-W. Shim, E-K. Suh, and C.J. Lee, Chem. Phys. Lett. **363,** 134 (2002).
23. Y-K. Tseng, I-N. Lin, K-S. Liu, T-S. Lin, and I-C. Chen, J. Mater. Res. **18,** 718 (2003).
24. JCPDS Card No. 36-1451 (Joint Committee for Powder Diffraction Standards, ASTM, Philadelphia, PA, 2000).
25. P. Yang, H. Yan, S. Mao, R. Russo, J. Johnson, R. Saykally, N. Morris, J. Pham, R. He, and H-J Choi, Adv. Func. Mater. **12,** 323 (2002).
26. K. Vanheusden, W.L. Warren, C.H. Seager, D.K. Tallant, J.A. Voigt, and B.E. Gnade, J. Appl. Phys. **79,** 7983 (1996).
27. J.M. Calleja and M. Cardona, Phys. Rev. B **16,** 3753 (1977).
28. F. Decremps, J. Pellicer-Porres, A.M. Saitta, J-C. Chervin, and A. Polian, Phys. Rev. B **65,** 092101 (2002).
29. L.X. Xu, S.P. Lau, J.S. Chen, G.Y. Chen, and B.K. Tay, J. Cryst. Growth **223,** 201 (2001).
30. Y. Dai, Y. Zhang, Q.K. Li, and C.W. Nan, Chem. Phys. Lett. **358,** 83 (2002); D.M. Bagnall, Y.F. Chen, Z. Zhu, T. Yao, S. Koyama, M.Y. Shen, and T. Goto, Appl. Phys. Lett. **73,** 1038 (1998).
31. Y.C. Kong, D.P. Yu, W. Fang, and S.Q. Feng, Appl. Phys. Lett. **78,** 407 (2001).
32. M.H. Huang, S. Mao, H. Feick, H.Q. Yan, Y.Y. Wu, H. Kind, E. Weber, R. Russo, and P.D. Yang, Science **292,** 1897 (2001).
33. Z.K. Tang, G.K.L. Wong, P. Yu, M. Kawasaki, A. Ohtomo, H. Koinuma, and Y. Segawa, Appl. Phys. Lett. **72,** 3270 (1998).
34. Y. Chen, N.T. Tuan, Y. Segawa, H.J. Jo, S.K. Hong, and T. Tao, Appl. Phys. Lett. **78,** 1469 (2001).
35. C. Liu, J.A. Zapien, Y. Yao, X. Meng, C.S. Lee, S. Fan, Y. Lifshitz, and S.T. Lee, Adv. Mater. **15,** 838 (2003).
36. E.I. Givargizov, J. Cryst. Growth **31,** 20 (1975).
37. J.Q. Hu, Q. Li, N.B. Wong, C.S. Lee, and S.T. Lee, Chem. Mater. **14,** 1216 (2002).
38. L. Brewer and D.F. Mastick, J. Phys. Chem. **19,** 834 (1951).
39. B.D. Yao, Y.F. Chan, and N. Wang, Appl. Phys. Lett. **81,** 757 (2002).
40. *Binary alloy phase diagrams,* 2nd ed., edited by T.B. Massalski, J.L. Murray, L.H. Bennett, and H. Baker (ASM, Metals Park, OH, 1990), Vol. 3, pp. 2938–2939.
41. L. Vayssieres, K. Keis, S-E. Lindquist, and A. Hagfeldt, J. Phys. Chem. B **105,** 3350 (2001).
42. R.A. Laudise, E.D. Kolb, and A.J. Caporaso, J. Am. Ceram. Soc. **47,** 9(1964); W-J. Li, E-W. Shi, W-Z. Zhong, and Z-W. Yin, J. Cryst. Growth **203,** 186 (1999).